Available online at www.sciencedirect.com
ScienceDirect
Bioorganic & Medicinal Chemistry 16 (2008) 2171–2182
Bioorganic & Medicinal Chemistry

A combined NMR and molecular dynamics simulation study to determine the conformational properties of agonists and antagonists against experimental autoimmune encephalomyelitis

Efthimia D. Mantzourani,[a,b] Klemen Blokar,[c] Theodore V. Tselios,[b] John M. Matsoukas,[b] James A. Platts,[d] Thomas M. Mavromoustakos[a,e] and Simona Golič Grdadolnik[c,*]

[a]*Institute of Organic and Pharmaceutical Chemistry, National Hellenic Research Foundation, 48 Vassileos Constantinou Avenue, 116 35, Athens, Greece*
[b]*Department of Chemistry, University of Patras, 265 00, Rion, Patras, Greece*
[c]*Laboratory for Molecular Modeling and NMR Spectroscopy, National Institute of Chemistry, Hajdrihova 19, SI-1001 Ljubljana, Slovenia*
[d]*Department of Chemistry, Cardiff University, CF10 3AT, Cardiff, Wales, UK*
[e]*Chemistry Department, University of Athens, Zographou 15784, Athens, Greece*

Received 5 September 2007; accepted 30 November 2007
Available online 1 January 2008

Abstract—Myelin basic protein (MBP) is one of the best characterized autoantigens causing multiple sclerosis (MS), via a procedure that involves a stable formation of the trimolecular complex of a T-cell Receptor (TCR), an MBP epitope, and the receptor HLA-DR2b. Experimental autoimmune encephalomyelitis (EAE) is considered as an instructive model for MS in humans, and plenty of X-ray data is available for a number of EAE inducing peptide-receptor complexes. To date, though, there are no data available for complexes involving peptides reversing EAE, namely antagonists. Conformational properties of the EAE inducing epitope MBP_{87-99} were analyzed in DMSO using the NOE connectivities and vicinal H^N–H^α coupling constants, and compared with the antagonist altered peptide ligands. A robust method, which is based on a combination of molecular dynamics and energy minimization, is proposed for identifying the putative bioactive conformations. Generated conformations are compared with the known X-ray structure of MBP_{83-96} (human sequence numbering) in the HLA-DR2b complex. The structural motif for the agonist–antagonist activity is discussed.
© 2008 Elsevier Ltd. All rights reserved.

1. Introduction

MS is a slowly progressive, immunologically mediated disease of the Central Nervous System (CNS), characterized by inflammation and demyelination of white matter in the brain and spinal cord.[1] In patients with MS the sheaths deteriorate to scleroses, which are hardened scars or plaques in multiple regions.[2] Investigations in recent decades indicate that MS is pathogenetically a T-cell mediated disease,[3] still retaining an elusive etiology but with a certitude that its development depends critically upon the interplay between environment and genetic factors. Experimental Autoimmune Encephalomyelitis (EAE) is a prototypic model for induced autoimmune diseases, considered as an instructive model for MS in humans. The role of T-cells in EAE has been substantiated by immunological approaches, proving that CD4+ T-helper (Th) cells are the primary disease inducing component. Th cells are activated upon recognition of an antigen after it is processed and presented, usually in the form of peptides, by cells expressing autologous class II molecules of Major Histocompatibility Complex (MHC). In the human, MHC molecules are referred to as HLA, an acronym for Human Leukocyte Antigens.[4]

Keywords: NMR; Molecular dynamics; Bioactive conformation; Agonist–antagonist activity.
* Corresponding author. Tel.: +386 1 4760409; fax: +386 1 4760300; e-mail: simona.grdadolnik@ki.si

0968-0896/$ - see front matter © 2008 Elsevier Ltd. All rights reserved.
doi:10.1016/j.bmc.2007.11.083

Although the antigenic components of myelin in MS have not been identified with certainty yet, myelin basic protein (MBP) is believed to be one of the main autoantigens and MBP_{87-99} is encephalitogenic in EAE.[5–9] A promising approach in the treatment of MS is the use of Altered Peptide Ligands (APLs) derived from the proteins of myelin sheath, mainly from the MBP.[10] The myelin-specific T-cells induce paralysis and demyelination when they are triggered by the native MBP. When these T cells recognize the APL they produce interleukin IL-4, which can reverse EAE. Clinical signs of EAE induced by MBP_{72-85} were completely suppressed by the linear APLs [Arg^{91}, Ala^{96}] MBP_{87-99} and [$Ala^{91,96}$] MBP_{87-99}.[11,12]

The 3D structures of the linear APLs [Arg^{91}, Ala^{96}] MBP_{87-99} and [$Ala^{91,96}$] MBP_{87-99} have already been described.[13,14] The studies were performed employing DMSO as a solvent, as it provides an amphiphilic environment, mimicking the physiological conditions at the receptor binding site.[15] The conformational analysis was based on a combination of Nuclear Magnetic Resonance (NMR) and molecular dynamics (MD) methods. Screening of MD generated conformations established populations with inter-atomic distances complying with the NMR data. Putative bioactive conformations have been proposed, that is, conformations that would enable binding with the HLA, but fail to activate the TCR and therefore to trigger an immune response. These conformations were further refined by extensive MD simulations at the receptor level.[16]

In these studies, the conformers within the conformational ensemble consistent with NMR data were found to have extended backbone topology, with turns formed in some of the populations. Interactions with the HLA-DR2b binding site did not change the overall extended topology of the linear antagonist APLs.[16] The outcome is intriguing as earlier analysis of the agonist MBP_{87-99} (Scheme 1) in DMSO suggested that one of the possible low energy conformers presented a topology with head-to-tail spatial proximity.[17] NMR and CD studies of the related polypeptide MBP fragment MBP_{81-98} in other chemical environments have shown that the immunodominant epitope of MBP (segment V_{86}–T_{95}) is forming a stable α-helix in a mixture of trifluoroethanol (TFA) and water and at membrane-mimetic conditions, while in aqueous solution the propensity for partially helical conformation in this segment is observed.[18] Recently, Hahn et al.[19] have reported the crystal structure (PDB code 1ymm) of the trimolecular complex of MBP_{83-96} (human sequence numbering), HLA-DR2b, and a human TCR. In this structure, the bound native peptide presents an extended conformation. For these reasons, in this work we have repeated the experiments on the agonist MBP_{87-99} in DMSO and performed the NMR measurements at higher magnetic field. In addition the analysis of MBP_{87-99} offers an opportunity to verify the validity of the methodology employed, as a direct comparison with crystallographic data and search for the bioactive conformation is possible.

2. Results and discussion

2.1. NMR characterization of MBP_{87-99} and comparison with the antagonistic APLs [Arg^{91}, Ala^{96}] MBP_{87-99} and [$Ala^{91,96}$] MBP_{87-99}

The proton and carbon chemical shifts of MBP_{87-99} (Table 1 in the supplementary material) have been assigned using the homonuclear (TOCSY, NOESY, and ROESY) and heteronuclear (^1H–^{13}C HSQC and ^1H–^{13}C HSQC–TOCSY) experiments. In the homonuclear 2D spectra additional peaks of lower intensity are observed, indicating the presence of small amounts of additional isomers. In the H^{α} region of ROESY spectra exchange cross-peaks of Pro^{96} and Pro^{99} resonances with the signals of the minor isomers appear. Pronounced sequential $d_{\alpha\alpha}$ NOE connectivities of Thr^{95}–Pro^{96} and Thr^{98}–Pro^{99} residues of minor isomers are indicating the *cis* orientation of the Thr–Pro peptide bonds in the minor isomers. However, according to the signal intensities the amount of *cis* isomers is lower than 10% and they were not further investigated. The C^{β} and C^{γ} chemical shifts of Pro residues of the major isomer and NOE connectivities observed between α protons of Thr^{95}/Thr^{98} and δ protons of Pro^{96}/Pro^{99} clearly confirm the *trans* orientation of the Thr–Pro peptide bonds in the major isomer. Small differences between C^{β} and C^{γ} chemical shifts of 4.7 and 4.2 ppm of the Pro^{96} and Pro^{99} observed in major isomer are typical for *trans* orientation of a X-Pro peptide bond.[20]

2.1.1. ^1H–^1H NOE connectivities. The proton–proton NOE connectivities have been collected from the NOESY spectrum measured at 75 ms at 800 MHz. The possible spin diffusion effects were investigated in NOESY spectra measured at different mixing times ranging from 50 to 150 ms. The intensity of most of the given NOE connectivities (Fig. 1) determined from the spectra measured at 50 and 75 ms differs by less than 5%. All connectivities which were reduced for more than 10% at shorter mixing time were excluded to avoid misinterpretation of NOE data due to spin diffusion effects.

Along the entire backbone of MBP_{87-99} both sequential NOE connectivities, $d_{\alpha N(i,\ i+1)}$ and $d_{NN(i,\ i+1)}$, are observed (Fig. 1), indicating conformational averaging between the β and α_R regions of ϕ, ψ conformational space.[21] The same conformational flexibility has been observed also for the linear antagonist APLs [Arg^{91}, Ala^{96}] MBP_{87-99} and [$Ala^{91,96}$] MBP_{87-99}.[13,14] The consecutive $d_{NN(i,\ i+1)}$ NOE connectivities are not indicative of the presence of populations with regular α-helical structure, because the diagnostic $d_{\alpha N(i,\ i+3)}$ or $d_{\alpha\beta(i,\ i+3)}$ connectivities[24] for such a local conformation are absent. These $d_{(i,\ i+3)}$ connectivities have been observed in NOESY spectra of a related MBP polypeptide fragment, MBP_{81-98}, for a stretch of residues between P_{85} and P_{96} in other chemical environments: aqueous solution, mixture of TFA and water, and membrane-mimetic environment.[18]

Absence of medium range (i, i+3) contacts and any of long range contacts is consistent with the presence of

H_2N-Val[87]-His[88]-Phe[89]-Phe[90]-Lys[91]-Asn[92]-Ile[93]-Val[94]-Thr[95]-Pro[96]-Arg[97]-Thr[98]-Pro[99]-OH

Scheme 1. Primary sequence of the agonist $MBP_{87–99}$ under study.

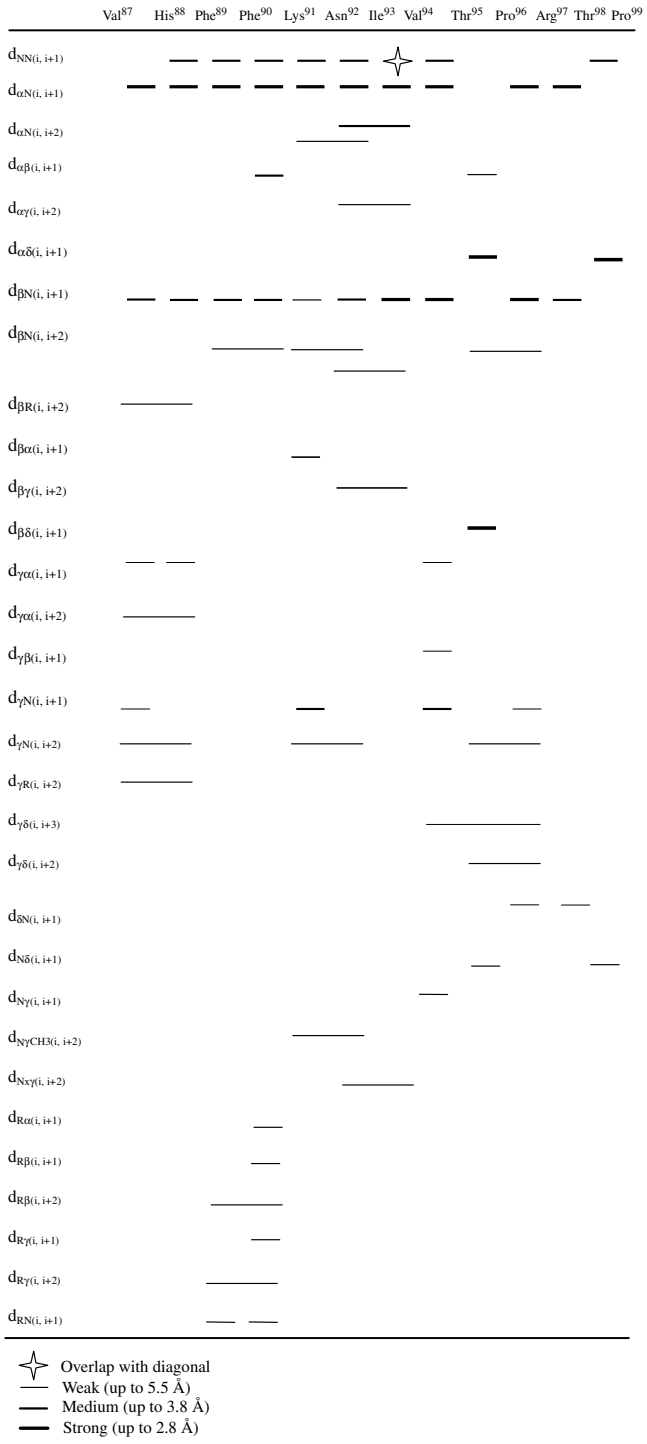

Figure 1. Intensities of observed inter-residue cross-peaks in the NOESY spectrum at mixing time of 75 ms in DMSO-d_6 at 25 °C and 800 MHz.

large amounts of populations of the $MBP_{87–99}$ with extended backbone conformation. Only in the central part of the $MBP_{87–99}$ backbone local folded structure can be identified. Inter-residue Asn[92] H^{α}–Val[94] H^{N} and Lys[91] H^{α}–Ile[93] H^{N} connectivities of medium and weak intensity indicate the presence of populations with β turns formed between the Lys[91]–Val[94] or Phe[90]–Ile[93] residues. On the basis of NOE intensities it can be speculated that the former turn is more frequently populated than the latter. The formation of turns in this region is in agreement with the temperature coefficients of amide protons (Table 1). The Ile[93] and Val[94] amide protons have the lowest temperature coefficients of −0.003 ppm/°C, which point to the partial participation of these two protons in the formation of intramolecular hydrogen bonds.[22,23] Typically, the amide proton of the fourth residue of the β turn forms a hydrogen bond with the carbonyl group of the first residue of the turn.[24] In our case the fourth residues of the two turns predicted on the basis of NOE connectivities are Ile[93] and Val[94].

The reduced overlap of side-chain methyl groups at higher magnetic field clarifies the assignment of NOE connectivities of these groups, which do not participate in any long-range contacts. Only medium range connectivities of side-chain methyl groups are observed (Fig. 1). Absence of long range NOE connectivities excludes the existence of populations with compact conformations possessing long range contacts including the previously proposed topology with the head-to-tail spatial proximity,[17] which resulted from the misinterpretation of the NOE connectivities of overlapped side-chain methyl groups at lower magnetic fields.

2.1.2. $^3J(H^N, H^{\alpha})$ coupling constants. Vicinal $^3J(H^N, H^{\alpha})$ coupling constants, which are related to the backbone angle ϕ through the well-known Karplus relation,[25] adopt in proteins typical values in the most populated conformations of the ϕ, ψ conformational space. The average $^3J(H^N, H^{\alpha})$ values of residues in the native β-sheet, P_{II}, and α_R-helix conformations, calculated from the experimental data deposited in BioMagResBank,[26] are 8.50, 5.24, and 5.07 Hz, respectively.[27] Similar results are obtained using high-resolution protein structures and the Karplus equation.[27] The difference in the average $^3J(H^N, H^{\alpha})$ values of a residue in the β-strand and P_{II} conformations and the β-strand and α_R-helix conformations is thus 3.26 and 3.43 Hz, respectively. This enables the application of the $^3J(H^N, H^{\alpha})$ couplings in differentiation of β ($\phi \approx -120°$, $\psi \approx 120°$) from the P_{II} ($\phi \approx -65°$, $\psi \approx 145°$) and α_R ($\phi \approx -60°$, $\psi \approx -40°$) conformations, but does not allow the differentiation between P_{II} and α_R conformations, which have similar angle ϕ. Note that β and P_{II} conformations are both located in the broad β region of the ϕ, ψ conformational space and both generate strong sequential $d_{\alpha N(i, i+1)}$ connectivity according to the similar angle ψ. It was shown that $^3J(H^N, H^{\alpha})$ coupling constants reflect the conformational propensities of different amino acid types.[28] Recently, these couplings have been used to differentiate between the conformational propensities of amino acid residues in conformationally very flexible systems like dipeptides[29] and fully denatured

Table 1. Temperature coefficients of amide protons of MPB_{87-99} in DMSO-d_6 in ppm/°C

Amino acid	His^{88}	Phe^{89}	Phe^{90}	Lys^{91}	Asn^{92}	Ile^{93}	Val^{94}	Thr^{95}	Arg^{97}	Thr^{98}
Temperature coefficient	−0.004	−0.004	−0.004	−0.005	−0.005	−0.003	−0.003	−0.007	−0.004	−0.006

ubiquitin.[27] This led us to the investigation of $^3J(H^N, H^\alpha)$ couplings in agonist MBP_{87-99} and the two linear antagonist APLs [Arg^{91}, Ala^{96}] MBP_{87-99} and [$Ala^{91,96}$] MBP_{87-99}.

Most of the $^3J(H^N, H^\alpha)$ couplings of the MBP_{87-99} lie in the region between 7.8 and 9 Hz (Fig. 2) and point to higher propensity of residues to adopt β than the P_{II} or α_R conformations. Evidently lower are only the couplings of Thr residues (7 Hz), which precede the Pro residues, indicating that Thr residues are less prone to the β conformation than other residues. The largest values of Ile^{93} and Val^{94} couplings (above 8.5 Hz) are not inconsistent with the formation of Lys^{91}–Val^{94} β turn, which was predicted on the basis of medium Asn^{92} H^α–Val^{94} H^N connectivity. Namely, the second and third residues of the type I β turn typically adopt the angles ϕ of $\approx -60°$ and $\approx -90°$.[24] According to the Karplus relation this would correspond to small coupling (≈5 Hz) of the second residue and large coupling (≈8 Hz) of the third residue in the turn. Indeed a slightly lower value of Asn^{92} coupling (7.4 Hz) is observed. On the other hand the formation of the Phe^{90}–Ile^{93} β turn predicted on the basis of weak Lys^{91} H^α–Ile^{93} H^N connectivity is not manifested in the coupling constants. It can be speculated that population with this turn is below the threshold that would observably affect the coupling constants. This is in accord with different intensities of the representative NOE connectivities, which indicate formation of the two turns, but do not satisfy the similarity of

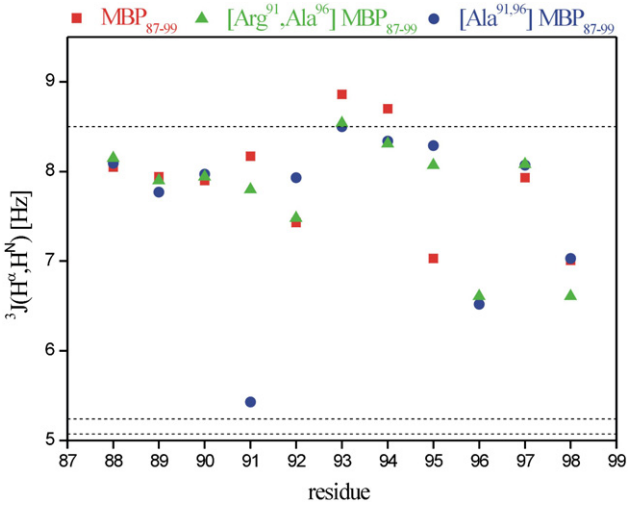

Figure 2. The $^3J(H^N, H^\alpha)$ coupling constants of the agonist MBP_{87-99} (square) and the two linear APLs [$Ala^{91,96}$] MBP_{87-99} (circle) and [Arg^{91}, Ala^{96}] MBP_{87-99} (triangle) measured in DMSO-d_6 at 25 °C and 600 MHz. The average $^3J(H^N, H^\alpha)$ values of residues found in the native β-sheet (8.50 Hz), P_{II} (5.24 Hz), and α_R-helix conformations (5.07 Hz) of proteins[27] are presented with the dashed lines.

Ile^{93} and Val^{94} NH temperature coefficients. However, the equal temperature coefficient of the Ile^{93} and Val^{94} amide protons can be a consequence of formation of hydrogen bonds with the Asn^{92} side chain. The carbonyl group of Asn side chain is known to make hydrogen bonds with peptide NH groups.

The antagonist APL [Arg^{91}, Ala^{96}] MBP_{87-99} reveals similar behavior regarding the coupling constants as the agonist MBP_{87-99}. The only significant difference is at the position 95, where coupling is increased by 1 Hz (Fig. 2). Obviously, the replacement of Pro^{96} with Ala^{96} increases the propensity of Thr^{95} for the β conformation. The Ala^{96} coupling is evidently lower and indicates that this residue is less prone to the β conformation than most of the other residues. The replacement of Lys with Arg at position 91 does not significantly affect the coupling constants. Investigation of NOE connectivities has shown that [Arg^{91}, Ala^{96}] MBP_{87-99} significantly occupies the extended conformation.[13] The local folded structure was predicted in the same region of the backbone as for the MBP_{87-99}, where the Asn^{92} H^α–$Val^{94}H^N$ connectivity was observed, which is indicative of formation of the Lys^{91}–Val^{94} β turn.

The coupling constants of the antagonist [$Ala^{91,96}$] MBP_{87-99} (Fig. 2) exhibit more deviations from the couplings of MBP_{87-99}. The replacement of Lys with Ala significantly affects the coupling constant at position 91. The Ala^{91} coupling of 5.4 Hz is the lowest observed in the three linear peptides and is in agreement with the NOE connectivities of [$Ala^{91,96}$] MBP_{87-99}.[14] Namely, the sequential $d_{\alpha N(i,\ i+1)}$ connectivity between residues Ala^{91} and Asn^{92} is completely absent. Thus the low value of Ala^{91} coupling corresponds to high propensity of this residue to adopt the α conformation. The formation of Lys^{91}–Val^{94} turn is not observed for this peptide,[14] consistent with the evident increase of Asn^{92} coupling. Due to the replacement of Pro^{96} with Ala^{96}, the Thr^{95} coupling is increased as observed for [Arg^{91}, Ala^{96}] MBP_{87-99}. [$Ala^{91,96}$] MBP_{87-99} also lacks the long range NOE connectivities and is proposed to adopt predominantly an extended conformation.[14]

The observed variations of structurally dependent NMR data along the agonist MBP_{87-99} and antagonists [Arg^{91}, Ala^{96}] MBP_{87-99}, [$Ala^{91,96}$] MBP_{87-99} backbone cannot be directly related to the biological activity of investigated peptides. Backbone conformational preferences of the residues at the N terminal part (87–90) interacting with the MHC molecules and T-cell receptor[13,14,19] are closely similar among the three peptides. The agonist–antagonist activity or antagonist potency cannot be attributed to the formation of local backbone structure in the central part of the peptides. Namely, the populations with turn conformation in the Asn^{92}–Val^{94} region

are observed for both, the agonist MBP_{87-99} and the antagonist [Arg^{91}, Ala^{96}] MBP_{87-99}, while they are absent in the case of the antagonist [$Ala^{91,96}$] MBP_{87-99}. The two antagonists possess similar inhibitory activity in the EAE assay. Thus also the significant difference in the backbone conformational preference and flexibility at position 91 between the antagonists is not affecting their biological profile.

2.2. Global behavior of MBP_{87-99} in the MD trajectories

2.2.1. Unrestrained molecular dynamics. The allowed lowest energy structures resulting from unrestrained molecular dynamics (trajectory I) were clustered according to their backbone dihedral angles into seven families (Fig. 3). Criteria for clustering were that (a) all conformers within each cluster should have dihedral angles that occupy the same region of the Ramachandran map, and that (b) RMSD of all structures within a cluster should present a deviation of less than 1 Å.

The RMSD when superimposing C^{α}, C^{β}, backbone C, and backbone N heavy atoms of the structures is 2.67 Å. Table 2 summarizes the parameters for the conformational ensemble. Conformational flexibility is evident, with the middle segment of the molecule forming turns in four out of the seven clusters. Cluster 3 presents a turn in the sequence His^{88}–Lys^{91}, while in clusters 5, 6, and 7 the turn is formed between residues Asn^{92} and Thr^{95}. The NH and C termini also present flexible molecular segments.

A series of snap-shots of the structure from the unrestrained MD at 5-ps intervals showed the variability of the structure and its tendency to form turns. At 200 ps a turn is formed in residues His^{88}–Lys^{91}, a feature present up to 250 ps, characterizing conformations in cluster 3. 300 ps later the turn is shifted in residues Asn^{92}–Thr^{95}, and it seems rather favorable, lasting for 350 ps and dominating clusters 5, 6, and 7. After 900 ps, the entire structure is extended, with no turns forming along the length of the peptide sequence.

The turns formed after unrestrained MD simulations are not fully consistent with the NMR data, because the typical $H^{\alpha}_{(2)}$–$NH_{(4)}$ NOEs that would indicate them are missing. $H^{\beta}_{(89)}$–$NH_{(91)}$ is observed, partially justifying the turn in cluster 3. The rest of the turns are shifted for one residue. The local structure, though, is still observed in the area depicted by the NOEs.

2.2.2. Backbone restrained MD. Dynamics run II, in which sequential $d_{NN(i,\ i+1)}$ distance constraints were used, resulted in a set of very compact conformations, even after unrestrained minimization. A variety of long-range NOE connectivities should be observed, if these conformations would contribute to the structural ensemble. None of them is present in NOESY spectra. Thus, these structures were not further analyzed.

For trajectory III, in which sequential $d_{\alpha N(i,\ i+1)}$ distance constraints were used, the RMSD when superimposing C^{α}, C, N, and O is 2.16 Å, presenting again conformational variation. Unrestrained minimization following dynamics simulation III provided low energy conformations. Figure 4 shows the lowest energy conformation of each of the seven clusters, derived after grouping them according to the same criteria mentioned above. The 2-ps intervals snap-shots were acquired, in an attempt to elucidate the structural variations throughout the simulation. The overall backbone conformation remains extended during simulation. No turns were formed whatsoever in this trajectory.

2.3. Backbone dihedral angles

The Ramachandran maps for all structures generated are included in supporting information.

2.3.1. Trajectory I. In cluster 1 the amino acid Thr^{95} occupies the α_L minimum of the Ramachandran map. All the rest have negative ϕ angle, occupying either the upper left region with positive ψ angle, or the lower left region with negative ψ angle. In accordance with the formation of turns, the middle two amino acids in each case have backbone ϕ angles from $-60°$ to $-75°$, and ψ angles within the region $0° \pm 30°$. The majority of the residues most frequently populate the ϕ angle around $-70°$, which would correspond to small values of coupling constants (~5 Hz). Thus the large values of measured coupling constants (Fig. 2) indicate low population of such conformations in DMSO.

2.3.2. Trajectory III. All the amino acids in the conformations resulting after trajectory III have backbone angles occupying the upper left quadrant of the ϕ, ψ plot with positive ψ angle, except Lys^{91} in cluster 1 that has a negative ψ angle, and thus satisfy the observation of strong sequential $d_{\alpha N(i,\ i+1)}$ connectivities.[30] In these conformations the Ile^{93}, Val^{94}, and Arg^{97} most frequently populate the β conformation and the Thr^{98} the P_{II} conformation, which is in accord with the values of coupling constant (Fig. 2). Namely the Ile^{93}, Val^{94}, and Arg^{97} have large values of coupling constants and Thr^{98} considerably smaller. The large couplings of residues 88 to 91 show less agreement with the calculated populations, where these residues to a large extent populate the ϕ angle around $-70°$.

2.4. Amide protons hydrogen bonds

It has been mentioned that the Ile^{93} and Val^{94} amide protons have the lowest temperature coefficients, suggesting that these two protons partially participate in the formation of intramolecular hydrogen bonds. After the MD simulations, though, no β turns were found to justify the above fact. The resulting conformations were subjected to a detailed analysis for the identification of other possible hydrogen bonds formed, where the amide protons of Ile^{93} or Val^{94} are involved (Table 3).

In almost all the clusters obtained after unrestrained MD, there was such a hydrogen bond (Table 4), whereas for backbone restrained MD, only cluster 2 presented one desired hydrogen bond. Therefore, there are indeed

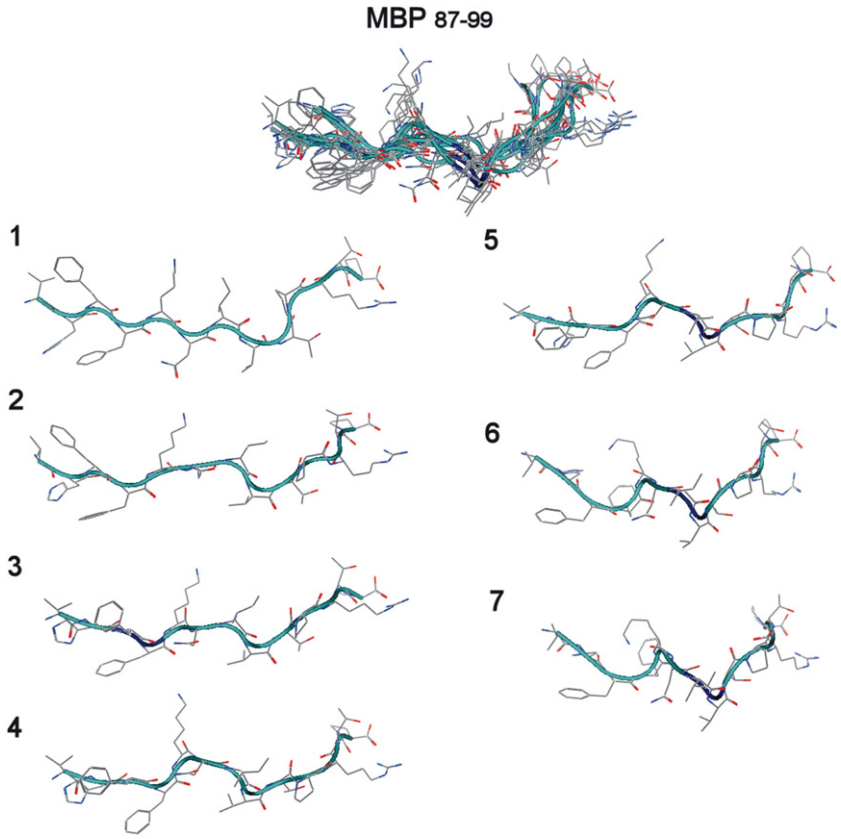

Figure 3. The ensemble of the conformers generated after applying unrestrained molecular dynamics to $MBP_{87–99}$, followed by energy minimization (top). The lowest energy conformation of each of the seven clusters in which conformers were divided to, according to their backbone dihedral angles (bottom). Backbone is colored blue when turns are present.

Table 2. Peptide parameters' report for the 7 families of conformations obtained after unrestrained molecular dynamics

Parameter	Observed		Expected	
	Mean	S.D.	Mean	S.D.
trans-Omega	169.3	7.8	180.0	5.8
C^{α} chirality	29.1	16.9	33.8	4.2
χ^1-gauche minus	−56.7	17.5	−66.7	15.0
χ^1-gauche plus	41.2	14.4	64.1	15.7
χ^1-*trans*	195.9	11.1	183.6	16.8
Helix ϕ	0.0	0.0	−65.3	11.9
Helix ψ	0.0	0.0	−39.4	11.3
χ^1-pooled s.d.	—	12.7	—	15.7
Proline ϕ	−60.2	10.2	−65.4	11.2

Included are the observed and expected values of the mean and standard deviation of various measured angles.

populations where the amide protons of Ile^{93} or Val^{94} form a hydrogen bond but none that would be indicative of them being the last residue of a β turn. Most of these hydrogen bonds are formed with the Asn^{92} side chain carbonyl group.

2.5. Consistence with NOE data

The distances that were already estimated experimentally from our NMR data were measured, in order to check if the obtained conformations could be considered as present in the solution ensemble. Histogram plots were obtained, to study the distribution of values. The values in each case were bucketed, and the number of counts per bucket was plotted. Values were normalized to correct for sample size and the results are displayed in percent. All histograms are included in supplementary data. Populations with interatomic distances complying with NMR data were identified. Percentages mentioned refer to the overall number of the selected structures in each run. Tables that present a summary of average measured distances and comparison with NOE connectivities obtained from NMR data are included in supplementary data. As can be observed, all clusters satisfy a range of the experimentally derived NOE distances and according to this criterion can be putatively as-

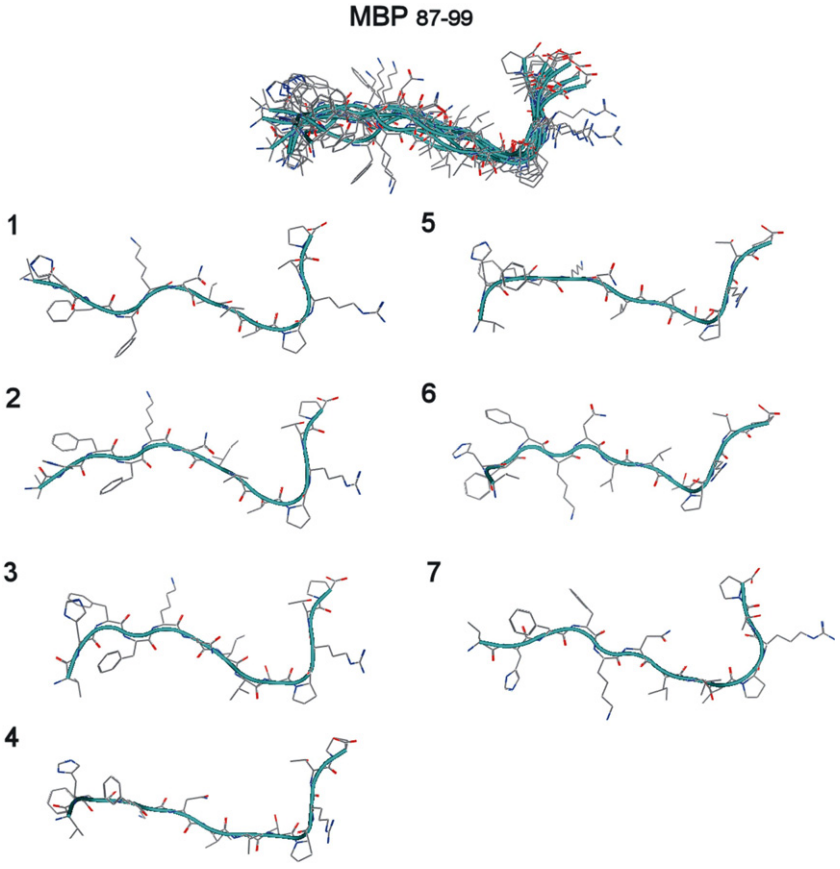

Figure 4. The ensemble of the conformers generated after backbone $d_{\alpha N(i,\ i+1)}$ restrained molecular dynamics to MBP_{87-99}, followed by energy minimization (top). The lowest energy conformation of each of the seven clusters in which conformers were divided to, according to their backbone dihedral angles (bottom).

Table 3. Peptide parameters' report for the 7 families of conformations obtained after unrestrained molecular dynamics

Parameter	Observed		Expected	
	Mean	S.D.	Mean	S.D.
trans-Omega	172.1	6.4	180.0	5.8
C^{α} chirality	28.2	18.7	33.8	4.2
χ^1-gauche minus	−55.1	15.6	−66.7	15.0
χ^1-gauche plus:	49.3	13.6	64.1	15.7
χ^1-*trans*	191.1	7.4	183.6	16.8
Helix ϕ	0.0	0.0	−65.3	11.9
Helix ψ	0.0	0.0	−39.4	11.3
χ^1-pooled s.d.	—	11.3	—	15.7
Proline ϕ	62.3	10.4	−65.4	11.2

Included are the observed and expected values of the mean and standard deviation of various measured angles.

Table 4. Hydrogen bonds in the resulting conformations after MD simulations, in which the amide protons of Ile^{93} or Val^{94} are involved

	Hydrogen bond atoms
$\mathbf{I}_1$	CO(91)–NH(93)
$\mathbf{I}_3$	COside(92)–NH(94)
$\mathbf{I}_4$	COside(92)–NH(94)
$\mathbf{I}_5$	COside(92)–NH(93)
$\mathbf{I}_6$	COside(92)–NH(94)
$\mathbf{I}_7$	COside(92)–NH(94)
$\mathbf{III}_2$	COside(92)–NH(94)

signed as present in the solution, in relative populations. However, the indicative NOE connectivities for formation of turns observed in several clusters resulting from unrestrained MD are absent. Thus these turns are not populated to an observable extent in DMSO.

Conformational flexibility is justified by the amount of NOE peaks present in the NOESY spectrum acquired, which could not all be satisfied in a unique conformation. This justifies the combination of molecular dynamics and energy minimization, as NMR could not identify

individual populations due to their fast interconvention rate. Nevertheless, NOESY spectra are sensitive enough for the identification of populations with local folded structures or compact structures with long-range contacts and can provide clues to the search of possible bioactive conformations. We have already applied the combination of molecular dynamics and energy minimization for the conformational analysis of linear APLs of $MBP_{87–99}$.[13,14] This study provides us with the opportunity to verify the validity of this combination, as a direct comparison with crystallographic data is possible.

2.6. Scan for the bioactive conformation

Hahn et al.[19] have reported the crystal structure (PDB code 1ymm) of the trimolecular complex of $MBP_{83–96}$, HLA-DR2b, and a human TCR by crystallography. The conformation of $MBP_{83–96}$ was isolated from the complex, and the segment 87–96 was used as a basis from which to identify a putative bioactive conformation from clusters generated after MD trajectories I and III. C_α RMSD from the X-ray structure was calculated in each case. Our threshold RMSD value for accepting a conformation as the bioactive was 1 Å. This search found that the lowest energy conformation from cluster 7 of trajectory III has C_α RMSD with the native peptide of 0.95 Å (Fig. 5). Side chains present a slightly different topology as seen, but this is expected as it is known that flexible molecules can be deformed when binding to proteins.[31] Therefore, this methodology can be established as a robust method for identifying putative bioactive conformations, even when X-ray data are absent. Theoretical methods arise as a solution for exploration of conformational space in the vicinity of conformers deduced from spectroscopic data and offer starting conformations for the conformational studies at the receptor binding site.

2.7. Comparison of putative bioactive conformations of the epitope $MBP_{87–99}$ with the antagonistic APLs [Arg^{91}, Ala^{96}] $MBP_{87–99}$ and [$Ala^{91,96}$] $MBP_{87–99}$

An overall comparison of the three structures reveals a heavy atom RMSD of 2.37 Å. In Figure 6, the backbones of the sequence 87–95 are shown, where $MBP_{87–99}$ has been colored red, [Arg^{91}, Ala^{96}] $MBP_{87–99}$ green, and [$Ala^{91,96}$] $MBP_{87–99}$ blue. The sequence 96–99 has been omitted for clarity, as residue Pro^{96} in the epitope leads to a bend in the conformation.

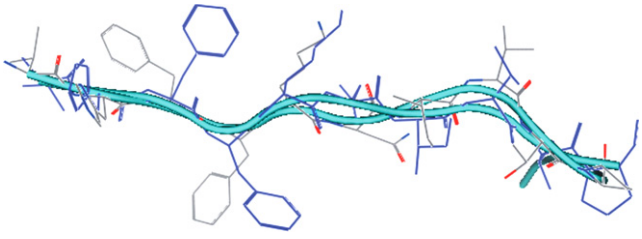

Figure 5. Superimposition of the sequence 87–95 of $MBP_{83–96}$ epitope isolated from the X-ray structure (pdb code 1ymm) (blue) and the bioactive one as identified after conformational analysis employing a combination of NMR and MOE molecular dynamics (grey). Cα RMSD for the two conformations is 0.95 Å.

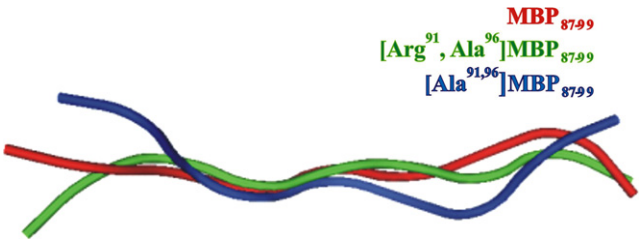

Figure 6. Superimposition of the putative bioactive conformations of $MBP_{87–99}$ (red) and the APLs [Arg^{91}, Ala^{96}] $MBP_{87–99}$ (green) and [$Ala^{91,96}$] $MBP_{87–99}$ (blue). Only the sequence 87–95 is shown for clarity.

The TCR involved in the X-ray structure reported by Hahn et al.[19] represents one of the best-characterized TCRs from a human autoimmune disease, and presents a topology notably different from that of antimicrobial ones.[32–34] Li et al.[35] have also isolated the complex of a human autoimmune TCR with HLA-DR2a. Both human autoimmune TCRs contact only the N-terminal region of the peptide rather than being centered on the peptide-MHC complex, with the one in complex with HLA-DR2b specifically contacting the residues P2 His^{88} and P3 Phe^{89}. The N-terminus of the peptide arches up at the TCR, which contacts the peptide at the Glu at position −4, that is, at the fourth amino acid before the first contact with the receptor. It is believed that the aberrant binding properties increase the probability that autoreactive T cells escape deletion in the thymus and attack self-myelin.

A two-step mechanism for TCR recognition and binding was proposed by Rudolph et al.[36] Initial TCR-MHC interactions, aided by minor contributions from TCR contacts with the peptide, guide the TCR to its ligand. The rigid CDR1 and CDR2 loops of the TCR are involved in this procedure. This is followed by a final folding of the two highly flexible CDR3 loops[37] of the TCR over the peptide. T-cell activation would be triggered only on the formation of stable peptide contacts. Thus, the TCR may scan MHC molecules using a 'lock and key' type of binding with its CDR1 and CDR2 loops, followed by an induced fit of its CDR3 loops over the peptide.[38]

From the above conformational analysis of $MBP_{87–99}$ we can see that the amino acids serving as TCR contacts in the trimolecular complex of TCR-peptide-HLA-DR2b, that is, His^{88} and Phe^{89}, have a different orientation in the antagonist analogues [Arg^{91}, Ala^{96}] $MBP_{87–99}$, and [$Ala^{91,96}$] $MBP_{87–99}$ compared with the agonist $MBP_{87–99}$. To quantify the relative change of the position of the imidazole His^{88} and phenyl Phe^{89} and Phe^{90} rings, we measured the angles and sides of the triangle formed by the centroids of the rings in their suggested putative bioactive conformations.

These triangles are shown in Figure 7, and the lengths of their sides and angles are presented in Table 5. Figure 8

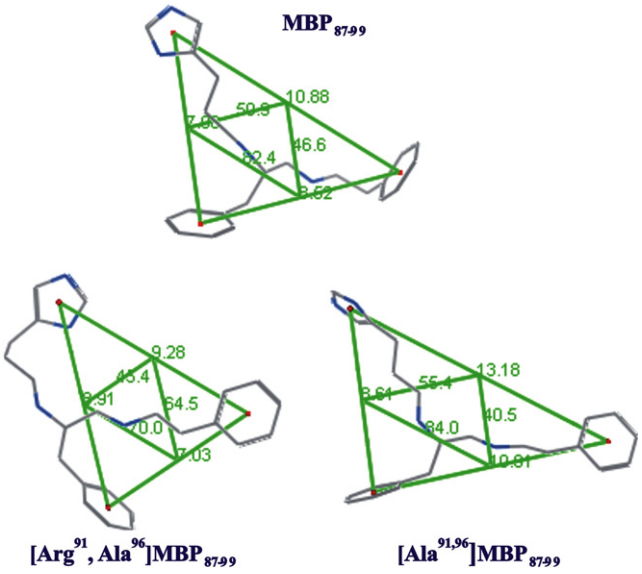

Figure 7. Triangles formed by ring centroids of His^{88}, Phe^{89} and Phe^{90}, for the putative bioactive conformations of MBP_{87-99}, [Arg^{91}, Ala^{96}] MBP_{87-99} and [$Ala^{91,96}$] MBP_{87-99}. Lengths of the sides and angles between the centroids are shown with green lines.

shows a superimposition of the sequence His^{88}–Phe^{90} for the three molecules. These data confirm that the orientation of rings in TCR anchor residues His^{88} and Phe^{89} has been altered substantially compared to the agonist APL, especially for [Arg^{91}, Ala^{96}] MBP_{87-99}, whereas HLA anchor residue Phe^{90} presents a similar topology. Even though the dihedrals χ_1 and χ_2 have such values that the ring is facing toward a different direction, they occupy a similar area in space. This is important as Phe^{90} tightly binds in P4 in the X-ray structure: hence, its conserved location may indicate binding in the same pocket on formation of the APL–HLA-DR2b complex.

In [Arg^{91}, Ala^{96}] MBP_{87-99} the ring of Phe^{89} shifts toward the binding groove and Phe^{90}, with a negative χ_2 dihedral angle. As a result, the distance between their centroids is smaller than in the native peptide. The same happens with the ring of His^{88}, which has a positive χ_1 dihedral angle, and again a smaller distance with the centroid of ring of Phe^{90}. In [$Ala^{91,96}$] MBP_{87-99} distances between the centroids of these rings are much bigger, due to a much higher value of χ_2 for His^{88}, which causes a different orientation of the imidazole ring, as well as the altered dihedrals χ_1 and χ_2 of Phe^{90} as mentioned above.

The altered orientation of the TCR contacts is important, as it may indicate a possible explanation for the analogues' biological activity. These APLs are EAE antagonists, and according to the definition of antagonism, they should form some interactions with the TCR, like agonists do, but much weaker. It is not exactly known what triggers an autoimmune T-cell response, but both trimolecular complexes isolated to date with autoreactive TCRs present a similar mode of binding: the TCR binds in a diagonal manner over the peptide-HLA complex. This may be the first step of binding, with the next step remaining elusive. In the APLs under study, the TCR contact residues are not available for interactions. Thus, the TCR probably approaches in that first step in a different mode, with a more centered orientation over receptor. This leads to different interactions formed and causes EAE antagonism.

The proposed mechanism of antagonist activity has been further seconded with recent results of MD simulations of antagonist APLs at the receptor level.[16] In these studies, the low energy DMSO structures of linear APLs [Arg^{91}, Ala^{96}]MBP_{87-99}, and [$Ala^{91,96}$]MBP_{87-99}[13,14] have been used as starting conformations. Interactions with HLA-DR2b have not affected the overall extended backbone topology of linear APLs. The orientation of side chains of the two TCR anchor residues, His^{88} and Phe^{89}, has changed in the receptor binding site, but remains significantly different from the orientation in the native peptide.[16] Several contacts of these two residues with deeply buried residues of the receptor are observed,[16] that are not present in the X-ray structure of native peptide.[19] Thus, they are no longer exposed outside the HLA-DR2b binding pocket and cannot contact the CD3 loops of TCR.

3. Conclusion

With the present extensive analysis of NOE connectivities at higher magnetic field we have shown that the agonist MBP_{87-99} preferably populates an extended conformation in DMSO, as has been observed for the two antagonistic APLs. Structural variations of the conformational ensemble are identified through the NMR data and MD simulations. However, the populations with the local folded structure observed for agonist and antagonist APLs cannot be related with their agonistic or antagonistic activity. There is no evidence for the existence of populations with a compact structure, due to the lack of long-range connectivities. Contrary to observations in other chemical environments[18] the populations with α-helical structure are not present in DMSO. Namely, the characteristic medium range NOEs indicative for formation of α-helix are not observed in DMSO.

X-ray data are available for an analogue of the peptide under study, in the form of a trimolecular complex with a human TCR and HLA-DR2b.[19] A search for a putative bioactive conformation, that is, a similar one to the crystallographic structure, was performed within all the resulting conformations from the Molecular Dynamics trajectories. Indeed a low energy conformation for the EAE inducing APL was identified, which has C_α RMSD with the native peptide of 0.95 Å, and similar orientation of the two TCR anchor residues His^{88} and Phe^{89} and the HLA anchor residue Phe^{90}. As explained, the altered topology of the TCR anchor residues in the two EAE reversing APLs may indicate a possible explanation for the analogues' biological activity. The low energy conformations of the antagonist APLs[13,14] obtained

Table 5. Geometries of triangles formed by centroids of rings of His[88], Phe[89], and Phe[90], for the X-ray structure of MBP_{83-96}, the putative bioactive conformations of epitope MBP_{87-99} and the antagonists [Arg^{91}, Ala^{96}] MBP_{87-99} and [$Ala^{91,96}$] MBP_{87-99}

	MBP_{83-96}	MBP_{87-99}	[Arg^{91}, Ala^{96}] MBP_{87-99}	[$Ala^{91,96}$] MBP_{87-99}
d (c88–c89)	7.92 Å	7.98 Å	8.91 Å	8.61 Å
d (c89–c90)	9.10 Å	8.52 Å	7.03 Å	10.91 Å
d (c90–c88)	10.88 Å	10.86 Å	9.28 Å	13.18 Å
a (c88–c90–c89)	45.7°	46.6°	54.4°	40.5°
a (c90–c88–c89)	55.2°	50.9°	45.4°	55.4°
a (c90–c89–c88)	79.2°	82.4°	70.0°	84.0°

d denotes the side length, *c* the ring centroid, and *a* the angle.

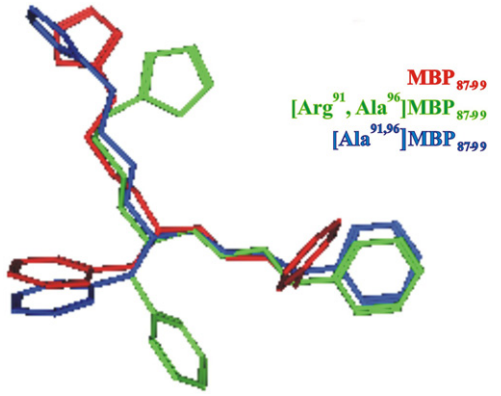

Figure 8. Superimposition of the sequence 88–90 of the putative bioactive conformations of MBP_{87-99} and the APLs [Arg^{91}, Ala^{96}] MBP_{87-99} and [$Ala^{91,96}$] MBP_{87-99}.

by the methodology described in this work have been used as starting conformations in MD studies at the receptor level,[16] which suggest different orientation of the two TCR anchor residues with respect to the native peptide. The side chains of these two residues are found to be buried in the interior of the HLA-DR2b receptor and cannot contact the TCR.[16]

These findings are of value, as they suggest that the methodology applied can be established as a robust method for identifying putative bioactive conformations, even when X-ray data are absent. It arises as a solution for exploration of conformational space in the vicinity of conformers deduced from spectroscopic data and offers starting conformations for the conformational studies at the receptor binding site.

4. Materials and methods

4.1. Synthesis of MBP_{87-99}

Linear epitope MBP_{87-99} was synthesized step by step using Fmoc/tBu methodology, that is, 2-chlorotrityl chloride (CLTR-Cl) resin (0.7 mmol Cl_/g) and Na-Fmoc (9-fluorenylmethyloxycarboxyl)-protected amino acids as previously described.[39] The purification and identification of peptide were achieved using reverse phase-high performance liquid chromatography (RP-HPLC) and electron spray ionization (ESI) mass spectroscopy, respectively.[40]

4.2. Nuclear magnetic resonance spectroscopy (NMR)

The high-resolution NMR spectra were recorded on Varian INOVA 600 MHz and Varian DirectDrive 800 MHz spectrometers at 25 °C in DMSO-d_6. The ^1H–^{13}C HSQC[41] and ^1H–^{13}C HSQC–TOCSY[41] experiments were performed with gradients. The TOCSY,[42] NOESY,[43], and ROESY[44] experiments were recorded using standard pulse sequences in the phase-sensitive mode. Typically, the 2D homonuclear proton spectra were acquired with a spectral width of 8012 Hz, 4096 data points in t_2, 8–32 scans, 512 complex points in t_1, and a relaxation delay of 1.5 s. The mixing time in ROESY and TOCSY experiments was 150 ms and 60 ms, respectively. The NOESY spectra were recorded with mixing time of 50, 75, 100, and 150 ms. Heteronuclear experiments were acquired with a ^1H spectral width of 6936 Hz, a ^{13}C spectral width of 20471 Hz, 1024 data points in t_2, and a relaxation delay of 1 s. The ^1H–^{13}C HSQC was recorded with 32 scans and 128 complex points in t_1. The ^1H–^{13}C HSQC–TOCSY was recorded with 128 scans, 256 complex points in t_1 and a mixing time of 32 ms.

Data were processed and analyzed with FELIX software package from Accelrys Software Inc. Spectra were zero-filled twice and apodized with a squared sine bell function shifted by $\pi/2$ in both dimensions. A linear prediction of the data was applied in ^{13}C dimension. Cross-peak volumes in NOESY spectra were calculated by integration routine within the FELIX software. A set of strong (up to 2.8 Å), medium (2.8–3.8 Å), and weak (3.8–5 Å) NOEs was established according to the integrated intensity of the geminal pair of protons β_1 and β_2 of Phe^{90}, which have a distance of 1.78 Å in all conformations.

Vicinal coupling constants $^3J(H^N, H^\alpha)$ were determined from the 1D ^1H spectra acquired at 25 °C. The coupling constants were measured from H^N resonances and a band-fitting algorithm was used to calculate the peak frequency of the H^N doublet. Spectra were processed without filter function to allow selection of the pure Lorentzian lineshape in the fitting procedure (Grams program, Thermo electron, San Jose, CA). Band frequencies, bandwidths, and intensities were allowed to vary simultaneously with no restrictions. The parameters determined in this way were tested by the fitting program based on the maximum entropy algorithm. The accuracy of the coupling constants is believed to be ±0.1 Hz.

4.3. Molecular modeling

All calculations were performed on an RM 3 GHz Pentium IV workstation using MOE 2005.06 by Chemical Computing Inc.[45] Molecular dynamics simulations were performed and the derived conformations were examined for consistency with experimental distance information designated by the obtained NOEs. Thus, populations of various conformers that represent local minima at the potential energy surface are identified.

4.3.1. Generating the starting conformation. AMBER94[46] force field was employed for all energy minimizations. An extended backbone structure of the peptide sequence was built, comprised of L-amino acids with standard parameters for all atom systems. The structure of the epitope was minimized using a succession of three methods: steepest descents (SD) algorithm to remove unfavorable steric contacts, then conjugate gradients to find its local minimum, followed by truncated Newton (TN). In all cases, energy convergence criterion is root mean square deviation (RMSD) force $\leqslant 0.001$ kcal mol^{-1} Å^{-1}.

4.3.2. Molecular dynamics studies. Three sets of MD[47–50] runs were performed using AMBER94[46] force field. Solvent DMSO was included into MD simulations via dielectric screening of the Coulombic term[46] in the AMBER94 force field. A dielectric constant of 45 was used. The macroscopic description of DMSO solvation appears in the literature[29,46,51–54] to perform adequately for the task in hand and also provides directly comparable data to our previous studies of antagonists.[13,14] The MD production runs were performed with a time step of 0.002 ps employing Verlet's algorithm,[55] for duration of 1 ns. An additional length of 100 ps heating time preceded the main simulation, to gradually heat the system from 1 to 298 K, for an effective simulation of the temperature of the NMR sample solution. Number of particles in the unit cell, volume, and temperature were held constant. All bond lengths involving hydrogens or lone pairs were constrained.

The first set of dynamics was completely unrestrained (I),[56] using a sampling period of 5 ps. Two sets of backbone restrained dynamics were performed, using a sampling period of 2 ps. Backbone distance constraints were employed to allow enough freedom to the side chains, so that sufficient sampling of conformational space could be obtained. Upper and lower bounds were used to establish a target interval. A weight factor representing the force constant (in kcal mol^{-1}) of 50 was chosen, to determine the strength of the restraint relative to the total energy of the molecule. A value of 50 was found to allow substantial deviation from the target interval in order to obtain a sufficient sampling, without raising significantly the total energy of the molecule. Sequential $d_{\mathrm{NN}(i,\ i+1)}$ distance constraints were used in the first set (II), in an attempt to obtain conformations within the α_{L} region of the Ramachandran map,[57] and sequential $d_{\alpha\mathrm{N}(i,\ i+1)}$ constraints were used in the second set (III), for sampling of the β region. All resulting conformations were subjected to a completely unrestrained energy minimization, following the same procedure described above, in order to make a direct comparison with the NMR results.

Selected structures had backbone dihedral angles ϕ and ψ within the core region of the Ramachandran map,[58,59] and trans ω dihedral angles.[60] The selected low energy structures were grouped into families according to their backbone dihedral angles and overall RMSD (in Å) when compared to the lowest energy structure of each run. For each cluster an RMSD of less than 1 Å was chosen.

Acknowledgments

Present work is supported by the Ministry of Development, Secretariat of Research and Technology of Greece (Grant EPAN YB/76) as well as the Slovenian–Greek bilateral project BI-GR/02-05-007.

Supplementary data

Table with ^{1}H and ^{13}C chemical shift assignment, NMR spectra, histogram plots and Ramachandran maps of data after MD runs, resulting conformations after dynamic run II, and tables of comparison of measured and calculated distances. Supplementary data associated with this article can be found, in the online version, at doi:10.1016/j.bmc.2007.11.083.

References and notes

1. Boccaccio, G. L.; Steinman, L. *J. Neurochem. Res.* **1996**, *45*, 647.
2. Tortora, G. J.; Grabowski, S. R. *Principles of Anatomy and Physiology*, 7th ed.; Harper Collins College publisher: New York, 1993, p. 439.
3. Martin, R.; McFarland, H. F.; McFarlin, D. E. *Ann. Rev. Immunol.* **1992**, *10*, 153.
4. The MHC sequence consortium, *Nature* **1999**, *401*, 921.
5. Steinman, L. *Neuron* **1999**, *24*, 511.
6. Zamvil, S. S.; Steinman, L. *Annu. Rev. Immunol.* **1990**, *8*, 579.
7. Ota, K.; Matsui, M.; Milford, E. L.; Mackin, G. A.; Weiner, H. L.; Hafler, D. A. *Nature* **1990**, *346*, 183.
8. Valli, A.; Sette, A.; Kappos, L.; Oseroff, C.; Sidney, J.; Miescher, G.; Hochberger, M.; Albert, E. D.; Adorini, L. *J. Clin. Invest.* **1993**, *91*, 616.
9. Martin, R.; Howell, M. D.; Jaraquemada, D.; Flerlage, M.; Richert, J.; Brostoff, S.; Long, E. O.; McFarlin, D. E.; McFarland, H. F. *J. Exp. Med.* **1991**, *173*, 19.
10. Mantzourani, E. D.; Mavromoustakos, T. M.; Platts, J. A.; Matsoukas, J. M.; Tselios, T. *Curr. Med. Chem.* **2005**, *12*, 1521.
11. Tselios, T.; Daliani, I.; Probert, L.; Deraos, S.; Matsoukas, E.; Roy, S.; Pires, J.; Moore, G.; Matsoukas, J. *Bioorg. Med. Chem.* **2000**, *8*, 1903.
12. Tselios, T.; Probert, L.; Daliani, I.; Matsoukas, E.; Troganis, A.; Gerothanassis, I.; Mavromoustakos, T.; Moore, G.; Matsoukas, J. *J. Med. Chem.* **1999**, *42*, 1170.
13. Mantzourani, E. D.; Tselios, T. V.; Golič Grdadolnik, S.; Brancale, A.; Platts, J. A.; Matsoukas, J. M.; Mavromoustakos, T. M. *J. Mol. Graphics Modell.* **2006**, *25*, 17.

14. Mantzourani, E. D.; Tselios, T. V.; Golič Grdadolnik, S.; Platts, J. A.; Brancale, A.; Deraos, G.; Matsoukas, J. M.; Mavromoustakos, T. M. *J. Med. Chem.* **2006**, *49*, 6683.
15. Soteriadou, K. P.; Tzinia, A. K.; Panou-Pamonis, E.; Tsikaris, V.; Sakarellos-Daitsiotis, M.; Sakarellos, C.; Papapoulou, Y.; Matsas, R. *Biochem. J.* **1996**, *313*, 455.
16. Mantzourani, E. D.; Platts, J. A.; Brancale, A.; Mavromoustakos, T. M.; Tselios, T. V. *J. Mol. Graphics Modell.* **2007**, *26*, 471.
17. Matsoukas, J.; Apostolopoulos, V.; Kalbacher, H.; Papini, A.; Tselios, T.; Chatzantoni, K.; Biagioli, T.; Lolli, F.; Deraos, S.; Papathanassopoulos, P.; Troganis, A.; Mantzourani, E.; Mavromoustakos, T.; Mouzaki, A. *J. Med. Chem.* **2005**, *48*, 1470.
18. Fares, C.; Libich, D. S.; Harauz, G. *FEBS J.* **2006**, *273*, 601.
19. Hahn, M.; Nicholson, M. J.; Pyrdol, J.; Wucherpfennig, K. W. *Nat. Immunol.* **2005**, *6*, 490.
20. Deber, C. M.; Madison, V.; Blout, E. R. *Acc. Chem. Res.* **1976**, *9*, 106.
21. Dyson, H. J.; Wright, P. E. *Annu. Rev. Biophys. Biophys. Chem.* **1991**, *20*, 519.
22. Kopple, K. D. *Biopolymers* **1971**, *10*, 1139.
23. Kessler, H. *Angew. Chem. Int., Ed. Engl.* **1982**, *21*, 512.
24. Wüthrich, K. *NMR of protein and nucleic acids*; John Wiley & Sons: New York, 1986, pp 126-127.
25. Karplus, M. *J. Chem. Phys.* **1959**, *30*, 11; Vuister, G. W.; Bax, A. *J. Am. Chem. Soc.* **1993**, *115*, 7772; Pardi, A.; Billeter, M.; Wüthrich, K. *J. Mol. Biol.* **1984**, *180*, 741; Ludvigsen, S.; Anderson, K. V.; Poulsen, F. M. *J. Mol. Biol.* **1991**, *217*, 731; Schmidt, J. M.; Blumel, M.; Lohr, F.; Ruterjans, H. *J. Biomol. NMR* **1999**, *14*, 1.
26. Seavey, B. R.; Farr, E. A.; Westler, W. M.; Markley, J. L. *J. Biomol. NMR* **1991**, *1*, 217.
27. Avbelj, F.; Golic Grdadolnik, S. *Protein Sci.* **2007**, *16*, 273.
28. Fiebig, K. M.; Schwalbe, H.; Buck, M.; Smith, L. J.; Dobson, C. M. *J. Phys. Chem.* **1997**, *100*, 2661.
29. Avbelj, F.; Golic Grdadolnik, S.; Grdadolnik, J.; Baldwin, R. L. *Proc. Natl. Acad. Sci. U.S.A.* **2006**, *103*, 1272.
30. Saulitis, J.; Lipins, E. *J. Magn. Reson.* **1990**, *87*, 80.
31. Nicklaus, M. C.; Wang, S.; Driscoll, J. S.; Milne, G. W. *Bioorg. Med. Chem.* **1995**, *3*, 411.
32. Garcia, K. C.; Degano, M.; Pease, L. R.; Huang, M.; Peterson, P. A.; Teyton, L.; Wilson, I. A. *Science* **1998**, *279*, 1166.
33. Stewat-Jones, G. B.; McMichael, A. J.; Bell, J. I.; Stuart, D. I.; Jones, E. Y. *Nat. Immunol.* **2003**, *8*, 403.
34. Hennecke, J.; Carfi, A. *EMBO J.* **2000**, *19*, 5611.
35. Li, Y.; Huang, Y.; Lue, J.; Quandt, J. A.; Martin, R.; Mariuzza, R. A. *EMBO J.* **2005**, *24*, 2968.
36. Rudolph, M. G.; Wilson, I. A. *Curr. Opin. Immunol.* **2002**, *14*, 1043.
37. Hare, B. J.; Wyss, D. F.; Osburne, M. S.; Kern, P. S.; Reinherz, E. L.; Wagner, G. *Nat. Struct. Biol.* **1999**, *6*, 574.
38. Willcox, B. E.; Gao, G. F.; Wyer, J. R.; Ladbury, J. E.; Bell, J. I.; Jakobsen, B. K.; van der Merwe, P. A. *Immunity* **1999**, *10*, 357.
39. Tselios, T.; Apostolopoulos, V.; Daliani, I.; Deraos, S.; Grdadolnik, S.; Mavromoustakos, T.; Melachrinou, M.; Thymianou, S.; Probert, L.; Mouzaki, A.; Matsoukas *J. Med. Chem.* **2002**, *45*, 275.
40. Tselios, T.; Daliani, I.; Deraos, S.; Thymianou, S.; Matsoukas, E.; Troganis, A.; Gerothanassis, I.; Mouzaki, A.; Mavromoustakos, T.; Probert, L.; Matsoukas, J. *Bioorg. Med. Chem. Lett.* **2000**, *10*, 2713.
41. Willker, W.; Leibfritz, D.; Kerssebaum, R.; Bermel, W. *Magn. Reson. Chem.* **1993**, *31*, 287.
42. Braunschweiler, L.; Ernst, R. R. *J. Magn. Reson.* **1983**, *53*, 521.
43. Jeener, J.; Meier, B. H.; Bachmann, P.; Ernst, R. R. *J. Chem. Phys.* **1979**, *71*, 4546.
44. Griesinger, C.; Ernst, R. R. *J. Magn. Reson.* **1987**, *75*, 261.
45. Chemical Computing Group Inc. 1010, Sherbrooke Street W, Suite 910; Montreal, Quebec; Canada H3A 2R7.
46. Cornell, W. D.; Cieplak, P.; Bayly, C. I.; Gould, I. R.; Merz, K.; Ferguson, D. M.; Spellmeyer, D. C.; Fox, T.; Caldwell, J. W.; Kollman, P. A. *J. Am. Chem. Soc.* **1995**, *117*, 5179.
47. Nikiforovich, G. V.; Vesterman, B. G.; Betins, J. *J. Biophys. Chem.* **1988**, *31*, 101.
48. Vesterman, B.; Saulitis, J.; Betins, J.; Liepins, E.; Nikiforovich, G. V. *Biochim. Biophys. Acta* **1989**, *998*, 204.
49. Ashish, A. G.; Kishore, R. *Eur. J. Biochem.* **2000**, *267*, 1455.
50. Galzitskaya, O.; Caflisch *J. Mol. Graphics Modell.* **1999**, *17*, 19.
51. Mavromoustakos, T.; Zervou, M.; Zoumpoulakis, P.; Kyrikou, I.; Benetis, N. P.; Polevaya, L.; Roumelioti, P.; Giatas, N.; Zoga, A.; Minakakis, P. M.; Kolocouris, A.; Vlahakos, D.; Golič Grdadolnik, S.; Matsoukas, J. *Curr. Top. Med. Chem.* **2004**, *4*, 445.
52. Zoumpoulakis, P.; Politi, A.; Golič Grdadolnik, S.; Matsoukas, J.; Mavromoustakos, T. *J. Pharm. Biomed. Anal.* **2006**, *40*, 1097.
53. Ashish, A. G.; Kishore, R. *Eur. J. Biochem.* **2000**, *267*, 1455.
54. Nagy, P. I.; Tejada, F. R.; Messer, W. S., Jr. *J. Phys. Chem. B* **2005**, *109*, 22588.
55. Verlet, L. *Phys. Rev.* **1967**, *159*, 98.
56. Ashish, A. G.; Kishore, R. *Eur. J. Biochem.* **2000**, *267*, 1455.
57. Ramachandran, G. N.; Ramakrishnan, C.; Sasisekharan, V. *J. Mol. Biol.* **1963**, *7*, 95.
58. Ramachandran, G. N.; Sasisekharan, V. *Adv. Protein Chem.* **1968**, *23*, 283.
59. Ramakrishnan, C.; Ramachandran, G. N. *Biophys. J.* **1965**, *5*, 909.
60. Laskowski, R.; McArthur, M.; Moss, D.; Thornton, J. *J. Appl. Crystallogr.* **1993**, *26*, 283.